

Contributions of anomalous large-scale circulations to the absence of tropical cyclones over the Western North Pacific in July 2020

Article

Accepted Version

Liu, H.-Y. ORCID: <https://orcid.org/0000-0002-7752-4553>, Gu, J.-F. ORCID: <https://orcid.org/0000-0002-7752-4553>, Wang, Y. and Xu, J. (2022) Contributions of anomalous large-scale circulations to the absence of tropical cyclones over the Western North Pacific in July 2020. *Geophysical Research Letters*, 49 (2). ISSN 0094-8276 doi: 10.1029/2021GL096652 Available at <https://centaur.reading.ac.uk/102369/>

It is advisable to refer to the publisher's version if you intend to cite from the work. See [Guidance on citing](#).

To link to this article DOI: <http://dx.doi.org/10.1029/2021GL096652>

Publisher: American Geophysical Union

All outputs in CentAUR are protected by Intellectual Property Rights law, including copyright law. Copyright and IPR is retained by the creators or other copyright holders. Terms and conditions for use of this material are defined in the [End User Agreement](#).

www.reading.ac.uk/centaur

CentAUR

Central Archive at the University of Reading

Reading's research outputs online

Contributions of Anomalous Large-Scale Circulations to the Absence of Tropical Cyclones over the Western North Pacific in July 2020

Hao-Yan Liu^{1,2}, Jian-Feng Gu³, Yuqing Wang^{4,*}, and Jing Xu²

¹College of Oceanography, Hohai University, Nanjing, China.

²State Key Laboratory of Severe Weather, Chinese Academy of Meteorological Sciences, China Meteorological Administration, Beijing, China.

³Department of Meteorology, University of Reading, Reading, United Kingdom.

⁴International Pacific Research Center and Department of Atmospheric Sciences, School of Ocean and Earth Science and Technology, University of Hawaii at Manoa, Honolulu, HI, USA

July 27, 2021 (submitted)
October 16, 2021 (resubmitted)
November 24, 2021 (first revised)
December 16, 2021 (second revised)
Dateline

Submitted to *Geophysical Research Letters*

*Corresponding author: Prof. Yuqing Wang, E-mail: yuqing@hawaii.edu

Key Points:

- No TC formed over the western North Pacific (WNP) in July 2020, an extreme month that has never occurred in history.
- It is due to the combination of anomalies in the WNP subtropical high, the South Asian high, the South Asian summer monsoon, and the TUTT.
- TC-resolving numerical experiments demonstrate the detrimental contributions of all the four large-scale atmospheric circulations.

This article has been accepted for publication and undergone full peer review but has not been through the copyediting, typesetting, pagination and proofreading process, which may lead to differences between this version and the [Version of Record](#). Please cite this article as doi: [10.1029/2021GL096652](https://doi.org/10.1029/2021GL096652).

This article is protected by copyright. All rights reserved.

Abstract

No tropical cyclone (TC) formed over the western North Pacific (WNP) in July 2020, which is record-breaking. Some recent studies suggested that this extreme event was mainly caused by the strong WNP subtropical high (WNPSH) in July 2020, which might not be the only reason. In this study, results from statistical and composite analyses indicate that the strong WNPSH, the strong South Asian high, the westward extended tropical upper-tropospheric trough, and the weak South Asian summer monsoon are all detrimental to TC genesis over the WNP and might contribute to the absence of TCs in July 2020. Results from sensitivity experiments using a regional atmospheric model that can resolve TCs further demonstrate that it was the collective effect, not any of the individual large-scale circulation anomalies, that induced the extremely unfavorable conditions for TC genesis and thus led to the record-breaking inactive TC month.

Keywords: tropical cyclone genesis, western North Pacific subtropical high, South Asian high, tropical upper-tropospheric trough, South Asian summer monsoon

Plain Language Summary

Tropical cyclones (TCs) become more active during the typhoon season (from July to September) over the western North Pacific (WNP). However, it is an exception in the records that no TC formed over the WNP in July 2020. Some recent studies suggest that this extreme event was mainly caused by the strong WNP subtropical high (WNPSH) in July 2020. This study identified four large-scale circulation anomalies that are detrimental to TC genesis over the WNP and might contribute to this extremely inactive TC event, including the strong WNPSH, the strong South Asian high, the westward extended tropical upper-tropospheric trough, and the weak South Asian summer monsoon. The strong WNPSH reduced the mid-level moisture and the low-level vorticity; the strong South Asian high and the westward shift of the tropical upper-tropospheric trough increased the deep-level vertical wind shear; and the weak South Asian summer monsoon could not provide sufficient low-level relative vorticity. It is the combined effect, not any of the individual large-scale circulation anomalies, that induced the extremely unfavorable conditions for TC genesis and led to the absence of TCs over the WNP in July 2020.

1. Introduction

Tropical cyclones (TCs) usually form over the western North Pacific (WNP) from July to September, often referred as the peak typhoon season. The annual mean WNP TC frequency is 3.8 in July during 1990–2020, and the largest TC count happened in 2017 (Fig. 1). It is well known that the favorable conditions for TC formation include warm sea surface temperature (SST), significant planetary vorticity, sufficient mid-level humidity, weak vertical wind shear (VWS), existing synoptic convective systems, and conditionally unstable atmosphere (Gray 1968). In the early summer 2020, the SST anomalies presented the La Niña pattern over the Pacific (Qiao et al. 2021; Wang et al. 2021; Zhou et al. 2021) with positive SST anomalies over the WNP that were beneficial to TC activity. However, no TC occurred in July 2020, which is the first event in the official records. Therefore, the inactive month might result from the extremely unfavorable atmospheric conditions.

During early summer 2020, the long-stalled Madden-Julian Oscillation was observed over the tropical Indian Ocean, which could cause the unfavorable background conditions for TC genesis over the WNP (Liu et al. 2021; Tian and Fan 2021). Besides, a few studies pointed out that the anomalously strong WNP subtropical high (WNPSH) was a dominant contributor to the absence of the WNP TC in July 2020 (Liu et al. 2021; Tian and Fan 2021; Wang et al. 2021a,b). The anomalous WNPSH in July 2020 was caused by the SST anomalies in the Indian, Pacific and Atlantic Oceans (Wang et al. 2021a,b), within which the tropical Indian Ocean played a crucial role (Wang et al. 2021a; Zhou et al. 2021). Tian and Fan (2021) found that the anomalously cooling in the Niño-4 region in May could also affect the WNPSH in July 2020. Wang et al. (2021a) suggested that the extremely strong WNPSH induced intense downward motion, dry middle troposphere, and weak low-level vorticity, and thus suppressed TC formation. Similar situations

also happened in July 1998 and 2010, with the anomalously strong WNPSH (Figs. S1 and 1a), but still several TCs formed. This strongly suggests that the WNPSH might not be the only dominant circulation system contributing to the absence of TCs in July 2020. Furthermore, in July 2017, the relatively stronger WNPSH (Fig. 1a) extended more westward and southward (Fig. 3e), but with the largest number of TCs in July on record. Another example is in July 2008 with only two TCs occurred over the WNP although the WNPSH was quite weak (Figs. 1a and 3d).

Previous studies (Tian and Fang 2021; Wang et al. 2021a; Zhou et al. 2021) explained the anomalies in large-scale circulations in summer 2020 using atmospheric general circulation models with horizontal resolutions of hundred kilometers, which are too coarse to resolve TCs. Higher resolution simulations that can resolve TC circulations and reproduce TC activities (Chang and Wang 2018; Shen et al. 2017) are necessary to examine whether the WNPSH was the only large-scale circulation system that inhibited TC genesis in July 2020 (Wang et al. 2021a) or any other large-scale circulation anomalies might also contribute to the extreme event.

Hence, this study aims to answer two questions: (1) in addition to the WNPSH, whether any other large-scale circulation anomalies might also independently or collectively contribute to the absence of TCs over the WNP in July 2020; and (2) can a high-resolution regional atmospheric model capture the extreme event and be used to evaluate the individual contributions by different large-scale circulation anomalies? The rest of the paper is organized as follows. Section 2 introduces data, methods and model. Section 3 analyzes the anomalous large-scale circulations related to the absence of TCs over the WNP in July 2020. The impacts of the identified large-scale circulations on TC activity are evaluated using a regional atmospheric model in Section 4. Finally, the main conclusions are summarized and discussed in Section 5.

2. Data and methods

2.1 Data and analysis methods

The TC best track dataset from 1990 to 2020 was obtained from the China Meteorological Administration (CMA) (Ying et al. 2014; Lu et al. 2021). The European Center for Medium Range Weather Forecasts (ECMWF) monthly reanalysis 5 (ERA5) with 0.25° horizontal resolution were used for the analysis of large-scale circulations and also for the initial and lateral boundary conditions for the numerical simulations. To facilitate the analysis, we defined the potential TC genesis region (PGR) as the region outlined in the dashed box in Fig. S2, in which all TC formed in July from 1990 to 2020. The location of TC formation is defined as where the TC first reached its maximum 10-m wind of 17 m s⁻¹ (8.3° N-28.5° N, 108.6° E-179.5° E). In addition, we defined active TC years with no less than 5 TCs (red bars in Fig. 1a) and inactive TC years with no more than 2 TCs (blue bars in Fig. 1a) in July, which are around the mean TC numbers plus or minus one standard deviation.

To explore the key factors inhibiting the WNP TC formation in July 2020, the genesis potential index (GPI, Emanuel and Nolan 2004) is used,

$$GPI = |10^5 \eta|^{3/2} \left(\frac{RH}{50}\right)^3 \left(\frac{V_{MPI}}{70}\right)^3 (1 + 0.1V_{shear})^{-2}, \quad (1)$$

where η is the 850-hPa absolute vorticity, RH is the 600-hPa relative humidity (RH), V_{MPI} is the maximum TC potential intensity (MPI, Emanuel 1995), V_{shear} is the magnitude of the environmental VWS between 200 and 850 hPa.

Indices of four large-scale circulations are defined as follows. The WNPSH index is defined by the regionally averaged geopotential height at 850 hPa over the climatological maximum interannual variability center (15°N-25°N, 115°E-150°E) as in Wang et al. (2013) and Huang et al. (2018). The SASM index is defined as the difference between the zonal wind anomalies averaged over (5°N-15°N, 90°E-130°E) and the zonal wind anomalies averaged over (22.5°N-32.5°N, 110°E-

140°E) at 850 hPa as in Wang and Fan (1999). The SAH index is defined by the geopotential height averaged over (20°N-27.5°N, 85°E-115°E) minus that over (27.5°N-35°N, 50°E-80°E) as in Wei et al. (2015). The TUTT index is defined as the westernmost longitude of the trough line at 200 hPa. The trough line is the zone where the zonal wind speed is less than 0.05 m s^{-1} and the vertical relative vorticity is greater than 10^{-5} s^{-1} .

2.2 Regional atmospheric model and experimental design

The advanced Weather Research and Forecasting (WRF) model version 3.8.1 (Skamarock et al. 2008) was used to understand the TC activities in extreme years, as in previous studies (e.g., Emanuel and Nolan 2004; Daloz et al. 2015; Chang and Wang 2018; Shen et al. 2017). The model was configured with 721×381 grid points, with the horizontal grid spacing of 12 km. The model had 30 vertical levels with the model top at 50 hPa. The model physics included Dudhia shortwave radiation scheme (Dudhia 1989), Rapid Radiative Transfer Model longwave radiation scheme (Mlawer et al. 1997), the Yonsei University planetary boundary layer (PBL) scheme (Hong et al. 2006), and the Kain–Fritsch cumulus parameterization scheme (Kain and Fritsch 1990). SST was interpolated from the ERA5 monthly averaged data and fixed throughout the simulations. To preserve the large-scale circulation feature, the large-scale spectral nudging method (Cha et al. 2011) was applied to both wind and temperature fields above the PBL with the wavelength larger than 1000 km and was conducted throughout the whole model domain and updated every 12 h. Five ensemble simulations were conducted for each experiment to test the robustness of finding based on reanalysis data. Impacts of individual large-scale circulations on TC activity in July 2020 were investigated through sensitivity numerical experiments. Details about the model setup and ensemble experiments can be found in Texts S1-S2 and Table S2.

3. Large-scale circulations responsible for TC absence in July 2020

3.1 GPI

GPI is a good starting point to identify the key large-scale environmental factors that possibly contributed to the absence of TCs over the WNP in July 2020, as it can reproduce seasonal TC genesis frequency and interannual variability in basin scales (Camargo et al. 2007). In comparison with the 31-year mean, the GPI presented negative anomalies over most of the PGR in July 2020, except the southwestern and northeastern portions (Fig. 2a). The regional mean GPI over TC formation locations was the lowest in July 2020 during 1990–2020 (Fig. S3a), similar to that shown in Wang et al. (2021a). The anomalies of MPI, mid-level RH, low-level relative vorticity and VWS with respect to the 31-year mean are examined (Figs. 2b-e) to understand the unfavorable environmental factors.

The positive GPI anomalies in the PGR were mainly caused by large MPI (Fig. 2b) due to the warm WNP associated with the La Niña pattern SST anomalies (Qiao et al. 2021; Wang et al. 2021a; Zhou et al. 2021). The mid-level RH was lower than the 31-year mean in the eastern portion of the PGR in July 2020 (Fig. 2c), and its regional mean was the lowest during 1990–2020 (Fig. S3c). The dry mid-troposphere is unfavorable for convective activity due to dry air entrainment and the associated melting and evaporative cooling. The anomalies of the mid-level RH closely correspond with the positive anomalies of the 500-hPa geopotential height. The low-level relative vorticity in July 2020 was lower than the 31-year mean in two portions of the PGR (Fig. 2d): one is located to the north of the PGR, and the other is located over the South China Sea (SCS) with anomalous easterlies. Its regional mean was the second lowest in recent 31-years (Fig. S3d). The VWS in July 2020 was larger than that of the 31-year mean in two portions of the PGR (Fig. 2e). As the low-level horizontal wind is generally weaker than that at the upper-level, the magnitude of the VWS mainly depends on the upper-level wind. The stronger VWS in the northwestern

portion of the PGR resulted from the anomalous northeasterly wind and that in the southern portion of the PGR was due to the anomalously stronger westerly wind at 200 hPa. Although not all GPI components were the most anomalous in July 2020, they together led to the lowest GPI during 1990–2020 (Figs. S4–S5). Therefore, the relatively drier mid-troposphere, weaker low-level relative vorticity, and stronger deep-layer VWS are the dominant large-scale environmental factors that could contribute to the absence of TCs over the WNP in July 2020. It is our interest to further examine the possible large-scale circulation systems that controls these unfavorable factors in the following subsection.

3.2 Large-scale circulation systems

According to the locations and features of the anomalous factors in GPI (Figs. 2c-e), we can speculate that the possible large-scale circulation systems could be the WNPSH (e.g., Wang and Wang 2019; Song et al. 2020), the South Asian summer monsoon (SASM) (e.g., Molinari and Vollaro 2013; Wang and Wang 2019; Zhao et al. 2019), the South Asian high (SAH) (e.g., Huang et al. 2011; Qu and Huang 2012; Wei et al. 2015; Wang and Wu 2016; Wang and Wang 2019; Wang and Wang 2021) and the tropical upper-tropospheric trough (TUTT) (Wu et al. 2015; Wang and Wang 2019; Zhao et al. 2019; Wang et al. 2020) based on their climatological characteristics. All the four large-scale circulations were found to affect the WNP TC activity in summer (Wang and Wang 2019). Composite analyses are used to verify whether the above systems were anomalous in July 2020. Here, we first compare the composite circulations of July in active and inactive TC years (red and blue bars in Fig. 1a) with the 31-year mean circulation to identify the most possible large-scale circulation systems that are important for TC activities in July. At low levels, the 31-year mean WNPSH circulation denoted by the 1520-gpm isoline (Fig. 3a) was larger in size than the mean in active TC years (ACTIVE; Fig. 3b) but smaller than the mean in inactive

TC years (INACTIVE; Fig. 3c). The anomalous geopotential heights also reflected the weaker (strong) WNPSH in active (inactive) TC years over the PGR (Fig. S6a,b). The 31-year mean SASM indicated by the monsoon westerly over the North Indian Ocean and SCS was stronger than the INACTIVE and weaker than the ACTIVE (Figs. 3a-c). This is consistent with previous studies that the sufficient relative vorticity in the monsoon trough favored TC activity (Frank 1987; McBride 1995; Harr and Chan 2005; Molinari and Vollaro 2013).

In the upper troposphere, the 31-year mean SAH indicated by the 12500-gpm isoline (Fig. 3g) was larger in size than the ACTIVE (Fig. 3h) and smaller than the INACTIVE (Fig. 3i). The anomalies of the 200-hPa geopotential height indicated that the SAH was weaker (stronger) in active (inactive) TC years over the northwestern portion of the PGR (Fig. S6f,g). The strong (weak) SAH in inactive (active) TC years enhanced (reduced) the northeasterly to the southeastern flank of the SAH and consequently enhanced (reduced) the VWS, since the low-level winds were prevailed by southwesterlies to the northwest of the WNPSH. Moreover, the 31-year mean TUTT (Fig. 3g) represented by the trough line shifted westward (eastward) in the active (inactive) TC years (Figs. 3h,i), accompanied with positive (negative) anomalies in 200-hPa geopotential height over the southern portion of the PGR (Figs. 70f,g). Recent studies (Wang and Wu 2016; Wang et al. 2020) suggested that TC formation was suppressed when the TUTT shifted westward, because the TUTT could cause not only the strong westerly VWS, but also the low RH and subsidence to the east of the trough axis. Therefore, the composite analyses suggest that few TCs occurred under the strong WNPSH and SAH, the weak SASM, and the westward shifted TUTT over the WNP in July.

A further comparison for July 2020 suggests that the strong WNPSH (Figs. 3f and S6e) may not be the only anomalous large-scale circulation system responsible for the absence of TCs (Wang

et al. 2021a). This is because besides the stronger WNPSH, the weaker SASM, the stronger SAH, and the more westwardly shifted TUTT simultaneously occurred in July 2020 (Figs. 3f,l and S6e,j) than the 31-year mean and INACTIVE (Figs. 3a,c,g,i and S6f,g). Thus, it can be inferred that the low mid-level RH (Fig. 2c) was associated with the strong WNPSH; the small low-level relative vorticity (Fig. 2d) was associated with the strong WNPSH and the weak SASM; and the large VWS (Fig. 2e) was associated with the strong SAH and the westwardly shifted TUTT in July 2020.

One may speculate that these large-scale circulation systems might be coupled together so that we can only focus on the strong WNPSH as in Wang et al. (2021a). Partial correlation analyses for the indices of the WNPSH, SASM, SAH and TUTT show that only the WNPSH and SASM are negatively correlated at statistically significant level (Table S1; Wang et al. 2013). However, it still could not conclude that the strong (weak) WNPSH must be accompanied with the weak (strong) SASM. This is further evidenced by two examples (Fig. S6). In July 2008 (inactive TC year), there were only two TCs over the WNP, but the WNPSH was weak (Figs. 3d and S6c). A possible reason may be related to the relatively weak SASM (Fig. 3d). On the contrary, the TC activity was the most active in July 2017 (activity TC year), but the WNPSH was stronger and larger than the 31-year mean and the ACTIVE (Figs. 3a,b; Fig. S6d). The negative impact of the WNPSH on TCs seemed to be offset by the strong SASM since most TCs occurred near the SCS where the SASM prevailed (Fig. 3e). Therefore, even though the large-scale circulation systems may not be independent, it is still worth investigating the individual contributions of the four large-scale circulation systems to TC formation, especially in extreme events.

The above hypothesis is first confirmed by statistical analyses of the correlation between the four large-scale circulation indices and TC frequency over the WNP in July during the 31 years. Figures 1a-d show the time series of indices of the WNPSH, SAH, SASM and TUTT and their

corresponding correlations with TC number in July. All the correlations are statistically significant at 95% confidence level except for the SAH. The total TC number negatively correlated with the WNPSH and SAH indices (Figs. 1a,b) and positively correlated with the SASM index and the westward location of the TUTT (Figs. 1c,d). Therefore, from the statistical perspective, the strong WNPSH and SAH, the weak SASM and the westward shift of the TUTT are unfavorable for TC activity over the WNP in July, which is consistent with the results of the composite analyses above. In July 2020, the four large-scale circulation systems all contributed negatively, inducing an extremely inadaptable environment to TC genesis over the WNP.

4. Results from numerical simulations and sensitivity experiments

The roles of the anomalous WNPSH, SAH, SASM and TUTT, and their relative importance to the absence of TCs over the WNP in July 2020 were further confirmed and examined based on two sets of high-resolution numerical simulations using the regional atmospheric model WRF (section 2.2). The first set of the experiments were performed to evaluate the ability of the model in reproducing the extremes in TC activity over the WNP in July 1994, 1998, 2017 and 2020, as these four years represent the most extreme events in July, either active with no less than 7 TCs (1994, 2017) or suppressed with no more than one TC (1998, 2020) according to the best track data (Fig. 1 and Table S3). The second set of experiments were performed to investigate the impacts of the four anomalous large-scale circulation systems identified in section 3 on the absence of TCs in July 2020. Four sensitivity experiments were conducted, including the weakened WNPSH (W_WNPSH), the weakened SAH (W_SAH), the weakened TUTT (W_TUTT), and the strengthened SASM (S_SASM), relative to their corresponding 31-year July mean (Fig. S7). The large-scale circulations were modified through the piecewise potential vorticity inversion and model dynamical adjustment (Text S3). A TC tracker algorithm was adopted to track TCs in the

model simulations (Text S4).

Results from the first set of experiments (Fig. 1e and Table S3) show that the model could well capture the TC activity in the selected extreme years although the ensemble-mean number of simulated TCs was slightly larger than that of the observed. It is the systemic bias of the model for TC climate simulation and some studies also found that the WRF model overrated TC frequency (e.g. Shen et al. 2017; Zhang and Wang 2017; Chang and Wang et al. 2018). The model captured the biggest number of TCs in 2017 and the smallest number of TCs in 2020. Moreover, one member could reproduce 0 TC in July 2020. Furthermore, results of the sensitivity experiments with the weakened WNPSH, SAH and TUTT, and the strengthened SASM were compared with those of the control experiment for July 2020 (CTRL) in the first set. Figure 4 shows the initial conditions of the CTRL and sensitivity experiments, together with the TC formation locations of all members in the corresponding July simulations. The monthly mean large-scale circulations of the model results (Figs. S8-S12) were similar to the initial conditions as the large-scale spectral nudging was adopted (Cha et al. 2011; Text S1). The simulated GPI in the four sensitivity experiments was larger than that in CTRL near the corresponding large-scale circulation region (Fig. S11). Compared with the CTRL run, the simulated TC numbers in W_WNPSH, W_SAH, W_TUTT, and S_SASM all increased (Figs. 1f and 4) with significant difference at the confidence level exceeding 90%. In W_WNPSH (Figs. 4b and S9a), more TCs formed in the central region of the PGR due to the increased low-level relative vorticity and the reduced downward motion associated with the weaker WNPSH. The VWS was also weakened to the northwest of the TC formation locations (Fig. S10a). In W_SAH (Figs. 4c and S10c), the weaker SAH induced the reduced VWS in the northwestern portion of the PGR so that more vortices in the central PGR could intensify to TCs during their westward movements. In W_TUTT (Figs. 4d and S10d), the

eastward shift of the TUTT reduced the VWS, causing more TCs forming to the west of the TUTT. In S_SASM (Figs. 4e and S9b), more TCs formed in the southwestern portion of the PGR, as the strengthened SASM featured with strong westerly winds enriched low-level relative vorticity for TC formation at low latitudes. Therefore, the concurrence of the stronger WNPSH, the stronger SAH, the more westwardly shifted TUTT, and the weaker SASM were responsible for and contributed about equally to the silent TC activity over the WNP in July 2020.

5. Conclusions and discussion

A record-breaking event with no TC formation occurred over the WNP in July 2020 for the first time. A few recent studies attributed this extreme event to the anomalous WNPSH, which was caused by the anomalies in SST in different tropical oceans. This study found that besides the WNPSH, the anomalous SASM, SAH and TUTT all played important roles in causing the quiet TC month over the WNP in July 2020. Weak low-level relative vorticity associated with the weak SASM and the strong WNPSH, low mid-level moisture associated with the strong WNPSH, and large VWS associated with the strong SAH and the TUTT, were all unfavorable for TC genesis (Fig. S13). This was revealed by the significant correlations between the four large-scale circulation indices and the July TC counts over the WNP. Furthermore, the high-resolution regional WRF model that can resolve the TCs was used to quantify the contributions of the four large-scale circulation anomalies. The model could reasonably reproduce four extreme years of TC activity in July over the last 31 years in the WNP. By replacing any of the four anomalous large-scale circulations by the 31-year July mean, the simulated TC numbers increased significantly, confirming the detrimental impacts of the anomalously strong WNPSH and SAH, westwardly shifted TUTT, and weak SASM on TC activity over the WNP. This demonstrates that it is the collective effect of the four large-scale circulation anomalies, not any of their individual

components that induced the unfavorable conditions to suppress TC genesis and thus led to the absence of TCs in July 2020. Results from this study strongly suggest that the indices of the four large-scale circulation systems could be considered in statistical models for TC seasonal forecasts, but with caution because the indices could not be linearly superimposed or composited because they are not all independent (Text S5 and Fig. S14). This study also suggests that good representation of relevant large-scale circulations is key to accurate forecasts of extreme events in TC activity over the WNP by numerical models.

The four anomalous large-scale circulations in July 2020 identified in this study were possibly related to the extremely warm tropical North Indian Ocean, the cold central Pacific Ocean, and the relatively warm tropical North Atlantic Ocean. Wang and Wu (2016) found that the TUTT shifted more westward when the negative SST anomalies occurred over the central Pacific (Text S6). A recent study by Zhou et al. (2021) suggested that the warm anomaly in the tropical North Indian Ocean favored the weak SASM and the strong WNPSH (Text S7). The strong SAH is also found to be related to the warm Indian Ocean (Huang et al. 2011; Qu and Huang 2012; Text S10). The correlation coefficients between the four large-scale circulation indices and SSTs supported the above views (Figs. S15-S17). In addition, the SAH is also affected by rainfall of the SASM (Wu et al. 2015), and the latter is closely related to the WNPSH (Wu and Chen 1998), which in turn follows the variation of the SAH (Jiang et al. 2011). However, the partial correlation analyses of the four indices indicated that only the WNPSH and SASM were significantly negatively correlated (Table S1). Therefore, the physical mechanisms for the simultaneous occurrence of the anomalous WNPSH, SAH, TUTT and SASM in July 2020 are complicated due to the involvement not only the air-sea interaction, but also the interaction among the large-scale circulation systems. This will be further investigated in a future study.

Acknowledgements

This study was supported in part by National Natural Science Foundation of China under grants 41730960 and 41805040, in part by the National Key R&D Program of China under grant 2017YFC1501602, and in part by “The Open Grants of the State Key Laboratory of Severe Weather” under grant 2021LASW-B10. Jian-Feng Gu is supported by the RevCon project, NE/N013743/1, and the ParaCon phase 2 project, NE/T003871/1, which are jointly funded by National Environment Research Council (NERC) and Met Office in United Kingdom. The authors are grateful to two anonymous reviewers for their constructive review comments and to Dr. Jianping Tang for suggestions of the numerical simulations.

Data availability

The ERA5 monthly analysis are available at <https://cds.climate.copernicus.eu/cdsapp#!/dataset/reanalysis-era5-pressure-levels-monthly-means?tab=form> and ERA5 monthly averaged data on single levels from 1979 to present (copernicus.eu). The best track data from CMA are available at http://tcdata.typhoon.org.cn/zjljsjj_zlhq.html. The simulation data are available at <https://zenodo.org/record/5800194#.YcP6BS0tZTZ> (DOI:10.5281/zenodo.5800194).

References

- Camargo, S.J., Emanuel, K.A., & Sobel, A.H. (2007), Use of a genesis potential index to diagnose ENSO effects on tropical cyclone genesis. *Journal of Climate*, 20, 4819-4834. <https://doi.org/10.1175/JCLI4282.1>.
- Cha, D. H., Jin, C. S, Lee, D. K., & Kuo, Y. H. (2011), Impact of intermittent spectral nudging on regional climate simulation using Weather Research and Forecasting model, *Journal of Geophysical Research-Atmospheres*, 116, D10103. <https://doi.org/10.1029/2010JD015069>.
- Cha, D.-H., & Wang, Y. (2013), A dynamical initialization scheme for real-time forecasts of tropical cyclones using the WRF Model, *Monthly Weather Review*, 141, 964-986. <https://doi.org/10.1175/MWR-D-12-00077.1>
- Chang, C. C., & Wang, Z. (2018), Relative impacts of local and remote forcing on tropical cyclone frequency in numerical model simulations. *Geophysical Research Letters*, 45, 7843–7850. <https://doi.org/10.1029/2018GL078606>.
- Daloz, A. S., & Coauthors (2015), Cluster analysis of downscaled and explicitly simulated North Atlantic tropical cyclone tracks. *Journal of Climate*, 28, 1333-1361. <https://doi.org/10.1175/JCLI-D-13-00646.1>.
- Davis, C. A. (1992), Piecewise potential vorticity inversion. *Journal of the Atmospheric Sciences*, 49, 1397–1411. [https://doi.org/10.1175/1520-0469\(1992\)049<1397:PPVI>2.0.CO;2](https://doi.org/10.1175/1520-0469(1992)049<1397:PPVI>2.0.CO;2)
- Dudhia, J. (1989), Numerical study of convection observed during the Winter Monsoon Experiment using a mesoscale two-dimensional model. *Journal of the Atmospheric Sciences*, 46, 3077–3107. [https://doi.org/10.1175/1520-0469\(1989\)046<3077:NSOCOD>2.0.CO;2](https://doi.org/10.1175/1520-0469(1989)046<3077:NSOCOD>2.0.CO;2).

- Emanuel, K. A. (1995), Sensitivity of tropical cyclones to surface exchange coefficients and a revised steady-state model incorporating eye dynamics. *Journal of the Atmospheric Sciences*, 52, 3969–3976. [https://doi.org/10.1175/1520-0469\(1995\)052<3969:SOTCTS>2.0.CO;2](https://doi.org/10.1175/1520-0469(1995)052<3969:SOTCTS>2.0.CO;2).
- Emanuel, K. A., & Nolan, D. S. (2004), Tropical cyclone activity and the global climate system. In: *Proceedings of the 26th Conference on Hurricanes and Tropical Meteorology*, American Meteorological Society, Miami, FL, 2004, 240–241. ftp://texmex.mit.edu/pub/emanuel/PAPERS/em_nolan_extended_2004.pdf.
- Feng, J., Chen, W., & Wang, X. (2020), Reintensification of the anomalous western North Pacific anticyclone during the El Niño Modoki decaying summer: relative importance of tropical Atlantic and Pacific SST anomalies. *Journal of Climate*, 33, 3271–3288. <https://doi.org/10.1175/JCLI-D-19-0154.1>
- Frank, W. M. (1987), Tropical cyclone formation. *A Global View of Tropical Cyclones*, Edited by R. Elsberry, et al., Nav. Postgrad. Sch., Monterey, Calif.
- Gray, W.M. (1968), Global view of the origin of tropical disturbances and storms. *Monthly Weather Review*, 96, 669-700. [https://doi.org/10.1175/1520-0493\(1968\)096<0669:GVOTOO>2.0.CO;2](https://doi.org/10.1175/1520-0493(1968)096<0669:GVOTOO>2.0.CO;2).
- Ham, Y.-G., Kug, J.-S., Park, J.-Y., & Jin, F.-F. (2013), Sea surface temperature in the north tropical Atlantic as a trigger for El Niño/Southern Oscillation events. *Nature Geoscience*, 6, 112-116. <https://doi.org/10.1002/2015G L063184>.
- Harr, P. A., & Chan, J. C. L. (2005), Monsoon impacts on tropical cyclone variability. *The Global Monsoon System: Research and Forecasting*, Edited by C. P. Chang, B. Wang and N. C. G. Lau, World Meteorological Organization, 512–542.
- Hong, S.-Y., Dudhia, J., & Chen, S.-H. (2004), A revised approach to ice microphysical processes for the bulk parameterization of clouds and precipitation. *Monthly Weather Review*, 132, 103–120. [https://doi.org/10.1175/1520-0493\(2004\)132<0103:ARATIM>2.0.CO;2](https://doi.org/10.1175/1520-0493(2004)132<0103:ARATIM>2.0.CO;2).
- Hong, S.-Y., & Lim, J.-O. (2006). The WRF single-moment 6-class microphysics scheme (WSM6). *Journal of the Korean Meteorological Society*, 42, 129–151.
- Huang, G., Qu, X., & Hu, K. M. (2011). The impact of the tropical Indian Ocean on the South Asian high in boreal summer. *Advances in Atmospheric Sciences*, 28, 421–432. <https://doi.org/10.1007/s00376-010-9224-y>.
- Huang, Y., Wang, B., Li, X., & Wang, H. (2018). Changes in the influence of the western Pacific subtropical high on Asian summer monsoon rainfall in the late 1990s. *Climate Dynamics*, 51(1-2), 443–455. <https://doi.org/10.1007/s00382-017-3933-1>
- Jiang, X., Li, Y., Yang, S., & Wu, R. (2011), Interannual and interdecadal variations of the South Asian and western Pacific subtropical highs and their relationship with the Asian-Pacific summer climate. *Meteorology and Atmospheric Physics*, 113, 171–180. <https://doi.org/10.1007/s00703-011-0146-8>.
- Kain, J. S., & Fritsch, J. M. (1990), A one-dimensional entraining/detraining plume model and its application in convective parameterization, *Journal of the Atmospheric Sciences*, 47, 2784–2802.
- Knutson, T. R., Sirutis, J. J., Garner, S. T., Held, I. M., Tuleya, R. E. (2007), Simulation of the recent multidecadal increase of Atlantic hurricane activity using an 18-km-grid regional model. *Bulletin of the American Meteorological Society*, 88, 1549–1565. <https://doi.org/10.1175/BAMS-88-10-1549>.
- Liu, C., Zhang, W., Jiang, F., Stuecker, M. F., & Huang, Z. (2021). Record low WNP tropical cyclone activity in early summer 2020 due to Indian Ocean warming and Madden-Julian

- Oscillation activity. *Geophysical Research Letters*, 48, e2021GL094578. <https://doi.org/10.1029/2021GL094578>
- Liu, H.-Y., & Tan, Z.-M. (2016), A dynamical initialization scheme for binary tropical cyclones. *Monthly Weather Review*, 144, 4787-4803, <https://doi.org/10.1175/MWR-D-16-0176.1>.
- Liu, H.-Y., Wang, Y., Xu, J., & Duan, Y. (2018) A dynamical initialization scheme for tropical cyclones under the influence of terrain. *Weather and Forecasting*, 33, 641-659. <https://doi.org/10.1175/WAF-D-17-0139.1>.
- Lu, X. Q., Yu, H., Ying, M., Zhao, B. K., Zhang, S., Lin, L. M., Bai, L. N., & Wan, R. J. (2021), Western North Pacific tropical cyclone database created by the China Meteorological Administration. *Advances in Atmospheric Sciences*, 38, 690–699. <https://doi.org/10.1007/s00376-020-0211-7>.
- Ma, L.-M., & Tan, Z.-M. (2009), Improving the behavior of the cumulus parameterization for tropical cyclone prediction: Convection trigger. *Atmospheric Research*, 92, 190-211. <https://doi.org/10.1016/j.atmosres.2008.09.022>.
- Mlawer, E. J., Taubman, S. J., Brown, P. D., Iacono, M. J., & Clough, S. A. (1997). Radiative transfer for inhomogeneous atmospheres: RRTM, a validated correlated-k model for the longwave. *Journal of Geophysical Research – Atmospheres*, 102, 16663–16682.
- McBride, J. L. (1995), Tropical cyclone formation. *Global Perspectives on Tropical Cyclones*, Edited by R. L. Elsberry, World Meteorological Organization, 63–105.
- Molinari, J., & Vollaro, D. (2013), What percentage of western North Pacific tropical cyclones form within the monsoon trough? *Monthly Weather Review*, 141, 499-505. <https://doi.org/10.1175/MWR-D-12-00165.1>.
- Nguyen, H. V., & Chen, Y.-L., 2011, High-resolution initialization and simulations of Typhoon Morakot (2009), *Monthly Weather Review*, 139, 1463-1491. <https://doi.org/10.1175/2011MWR3505.1>
- Panofsky, H. A., & Brier, G. W. (1968), Some applications of statistics to meteorology. *The Pennsylvania State University*, 224 pp.
- Qiao, S., Chen, D., Wang, B., Cheung, H.-N., Liu, F., Cheng, J., Tang, S., Zhang, Z., Feng, G. & Dong, W. (2021). The longest 2020 Meiyu season over the past 60 years: Subseasonal perspective and its predictions. *Geophysical Research Letters*, 48, e2021GL093596. <https://doi.org/10.1029/2021GL093596>.
- Qu, X., & Huang, G., (2012). An enhanced influence of tropical Indian Ocean on the South Asia High after the late 1970s. *Journal of Climate*, 25, 6930-6941. <https://doi.org/10.1175/JCLI-D-11-00696.1>.
- Shen, W., Tang, J., Wang, Y., Wang, S., & Niu, X. (2017), Evaluation of WRF model simulations of tropical cyclones in the western North Pacific over the CORDEX East Asia domain. *Climate Dynamics*, 48, 2419-2435. <https://doi.org/10.1007/s00382-016-3213-5>.
- Skamarock, W. C., Klemp, J. B., Dudhia, J., Gill, D. O., Barker, D. M., Duda, M. G., et al. (2008), A description of the Advanced Research WRF version 3. *NCAR Technical Notes*, Note NCAR/TN-475+STR, 113pp. <http://dx.doi.org/10.5065/D68S4MVH>.
- Song, J., Klotzbach, P. J., & Duan, Y. (2020), Differences in western north Pacific tropical cyclone activity among three El Niño phases. *Journal of Climate*, 33, 7983-8002. <https://doi.org/10.1175/JCLI-D-20-0162.1>.
- Tao, W.-K., Simpson, J., & McCumber, M. (1989), An ice-water saturation adjustment. *Monthly Weather Review*, 117, 231–235.
- Thompson, G., Field, P. R., Rasmussen, R. M. & Hall, W. D. (2008), Explicit forecasts of winter

- precipitation using an improved bulk microphysics scheme. Part II: Implementation of a new snow parameterization. *Monthly Weather Review*, 136, 5095–5115. <https://doi.org/10.1175/2008MWR2387.1>.
- Tian, B., & Fan, K. (2021), Absence of tropical cyclone genesis over the western North Pacific in July 2020 and its prediction by CFSv2. *Frontiers in Earth Science*. 9:771172. <https://doi.org/10.3389/feart.2021.771172>
- Wang, B., Xiang, B., & Lee, J. Y. (2013), Subtropical High predictability establishes a promising way for monsoon and tropical storm predictions. *Proceedings of the National Academy of Sciences of the United States of America*, 110, 2718-2722. <https://doi.org/10.1073/pnas.1214626110>.
- Wang, B., & Fan Z. (1999), Choice of South Asian summer monsoon indices. *Bulletin of the American Meteorological Society*, 80, 629–638. [https://doi.org/10.1175/1520-0477\(1999\)080<0629:COSASM>2.0.CO;2](https://doi.org/10.1175/1520-0477(1999)080<0629:COSASM>2.0.CO;2).
- Wang, C., & Wang, B. (2019), Tropical cyclone predictability shaped by western Pacific subtropical high: integration of trans-basin sea surface temperature effects. *Climate Dynamics*, 53, 2697-2714, <https://doi.org/10.1007/s00382-019-04651-1>.
- Wang, C., & Wang, B. (2021), Impacts of the South Asian high on tropical cyclone genesis in the South China Sea. *Climate Dynamics*, 56, 2279-2288. <https://doi.org/10.1007/s00382-020-05586-8>
- Wang, C., & Wu, L. (2016), Interannual shift of the tropical upper-tropospheric trough and its influence on tropical cyclone formation over the western North Pacific. *Journal of Climate*, 29, 4203–4211. <https://doi.org/10.1175/JCLI-D-15-0653.1>.
- Wang, C., Wu, K., Wu, L., Zhao, H., & Cao, J. (2021a), What caused the unprecedented absence of western North Pacific tropical cyclones in July 2020? *Geophysical Research Letters*, 48, e2020GL092282. <https://doi.org/10.1029/2020GL092282>.
- Wang, C., Yao, Y., Wang, H., Sun, X., & Zheng, J. (2021b), The 2020 summer floods and 2020/21 winter extreme cold surges in China and the 2020 typhoon season in the western North Pacific. *Advances in Atmospheric Sciences*, 38, 896–904, <https://doi.org/10.1007/s00376-021-1094-y>.
- Wang, H., & Wang, Y. (2014), A numerical study of typhoon Megi (2010). Part I: Rapid intensification. *Monthly Weather Review*, 142, 29-48. <https://doi.org/10.1175/MWR-D-13-00070.1>.
- Wang, H., Wang, Y., & Xu, H.-M. (2013), Improving simulation of a tropical cyclone using dynamical initialization and largescale spectral nudging: A case study of Typhoon Megi (2010). *Acta Meteorologica Sinica*, 27, 455-475. <https://link.springer.com/article/10.1007/s13351-013-0418-y>.
- Wang, Z., Zhang, G., Dunkerton, T. J., & Jin., F.-F. (2020), Summertime stationary waves integrate tropical and extratropical impacts on tropical cyclone activity. *Proceedings of the National Academy of Sciences of the United States of America*, 37, 22720-22726. <https://www.pnas.org/lookup/suppl/doi:10.1073/pnas.2010547117/-/DCSupplemental>.
- Wei, W., Zhang, R., Wen, M., Kim, B.-J., & Nam, J.-C. (2015). Interannual variation of the South Asian high and its relation with Indian and East Asian summer monsoon rainfall. *Journal of Climate*, 28(7), 2623–2634. <https://doi.org/10.1175/jcli-d-14-00454.1>
- Wu, C. C., & Emanuel, K. A. (1995a), Potential vorticity diagnostics of hurricane movement. Part I: A case study of Hurricane Bob (1991). *Monthly Weather Review*, 123, 69–92. [https://doi.org/10.1175/1520-0493\(1995\)123<0069:PVDOHM>2.0.CO;2](https://doi.org/10.1175/1520-0493(1995)123<0069:PVDOHM>2.0.CO;2).

- Wu, C. C., & Emanuel, K. A. (1995b), Potential vorticity diagnostics of hurricane movement. Part II: Tropical storm Ana (1991) and Hurricane Andrew (1992). *Monthly Weather Review*, *123*, 93–109. [https://doi.org/10.1175/1520-0493\(1995\)123<0093:PVDOHM>2.0.CO;2](https://doi.org/10.1175/1520-0493(1995)123<0093:PVDOHM>2.0.CO;2).
- Wu, C. C., Huang, T. S., Huang, W. P., & Chou, K. H. (2003), A new look at the binary interaction: Potential vorticity diagnosis of the 697 unusual southward movement of Tropical Storm Bopha (2000) and its interaction with Supertyphoon Saomai (2000). *Monthly Weather Review*, *131*, 1289–1300. [https://doi.org/10.1175/1520-0493\(2003\)131<1289:ANLATB>2.0.CO;2](https://doi.org/10.1175/1520-0493(2003)131<1289:ANLATB>2.0.CO;2).
- Wu, G., He, B., Liu Y., Bao, Q., & Ren, R. (2015), Location and variation of the summertime upper-troposphere temperature maximum over South Asia. *Climate Dynamics*, *45*, 2757–2774. <https://doi.org/10.1007/s00382-015-2506-4>.
- Wu, R., & Chen, L. (1998), Decadal variation of summer rainfall in the Yangtze-Huaihe River valley and its relationship to atmospheric circulation anomalies over East Asia and western North Pacific. *Advances in Atmospheric Sciences*, *15*, 510–522. <https://doi.org/10.1007/s00376-998-0028-2>.
- Ying, M., Zhang, W., Yu, H., Lu, X., Feng, J., Fan, Y., Zhu, Y., & Chen, D. (2014), An overview of the China Meteorological Administration tropical cyclone database. *Journal of Atmospheric and Oceanic Technology*, *31*, 287-301. <https://doi.org/10.1175/JTECH-D-12-00119.1>.
- Zhang, C., & Wang, Y. (2017), Why is the simulated climatology of tropical cyclones so sensitive to the choice of cumulus parameterization scheme in the WRF model? *Climate Dynamics*, *51*, 3613–3633. <https://doi.org/10.1007/s00382-018-4099-1>.
- Zhang, F., D. Tao, Y. Q. Sun, and J. D. Kepert (2017), Dynamics and predictability of secondary eyewall formation in sheared tropical cyclones, *Journal of Advances in Modeling Earth Systems*, *9*, 89–112, <https://doi.org/10.1002/2016MS000729>.
- Zhao, H., Chen, S., & Klotzbach, P. J. (2019), Recent strengthening of the relationship between the western north Pacific monsoon and western north Pacific tropical cyclone activity during the boreal summer. *Journal of Climate*, *32*, 8283–8299. <https://doi.org/10.1175/JCLI-D-19-0016.1>.
- Zhou, Z. Q., Xie, S. P., & Zhang, R. (2021), Historic Yangtze flooding of 2020 tied to extreme Indian Ocean conditions. *Proceedings of the National Academy of Sciences of the United States of America*, *118*, e2022255118. <https://doi.org/10.1073/pnas.2022255118>.

Figure captions:

Figure 1. (a-d) Time series of the TC numbers (bars) from the best-track TC data over the WNP in July and the detrended normalized indices (black lines) of the WNPSH, SAH, SASM, and TUTT, respectively, in July from 1990 to 2020, with their correlation coefficients given at the top of their corresponding panels. The star after the correlation coefficient means the correlation exceeds 95% confidence level. The red (blue) bars denote the active (inactive) TC years. (e) TC counts of July from the best track data (red) and ensemble-mean model results (blue) in 1994, 1998, 2017, and 2020, respectively. (f) TC counts from ensemble-mean model results in the experiments of CTRL, W_WNPSH, W_SAH, W_TUTT and S_SASM in July 2020. The thin vertical bars in (e-f) are the ensemble range.

Figure 2. Differences in (a) GPI, (b) MPI (m s^{-1}), (c) 600-hPa RH (shading, %) and 500-hPa geopotential height (contours, 10 gpm), (d) 850-hPa relative vorticity (shading, 10^{-6} s^{-1}) and 850-hPa horizontal winds (vectors, m s^{-1}), and (e) VWS (shading, m s^{-1}) and 200-hPa horizontal winds (vectors, m s^{-1}) between July 2020 and the 31-year July mean. The dashed blue box denotes the potential genesis region (PGR).

Figure 3. Geopotential height greater than 1520 gpm (contours, 10 gpm), zonal wind speed (shading, m s^{-1}), and horizontal winds (vectors, m s^{-1}) at 850 hPa in July for (a) the 31-year mean, (b) mean active TC years (ACTIVE), (c) mean inactive TC years (INACTIVE), (d) 2008, (e) 2017 and (f) 2020. (g-l) are the same as (a-f) but for geopotential height (contour and shading, 10 gpm) and horizontal winds (vectors, m s^{-1}) at 200 hPa. The red dots denote the locations of TC formation. The green line represents the trough line of TUTT. The dashed blue box denotes the PGR.

Figure 4. Initial conditions of the WRF model in (a) CTRL, (b) W_WNPSH, (c) W_SAH, (d) W_TUTT, and (e) S_SASM, including horizontal wind with zonal wind greater than 1 m s^{-1} (vectors, m s^{-1}) and geopotential height greater than 1520 gpm (contours, 10 gpm) at 850 hPa, and geopotential height at 200 hPa (shading, 10 gpm). The dashed blue box denotes the PGR. The red dots are the locations of the simulated TC formation in all members.

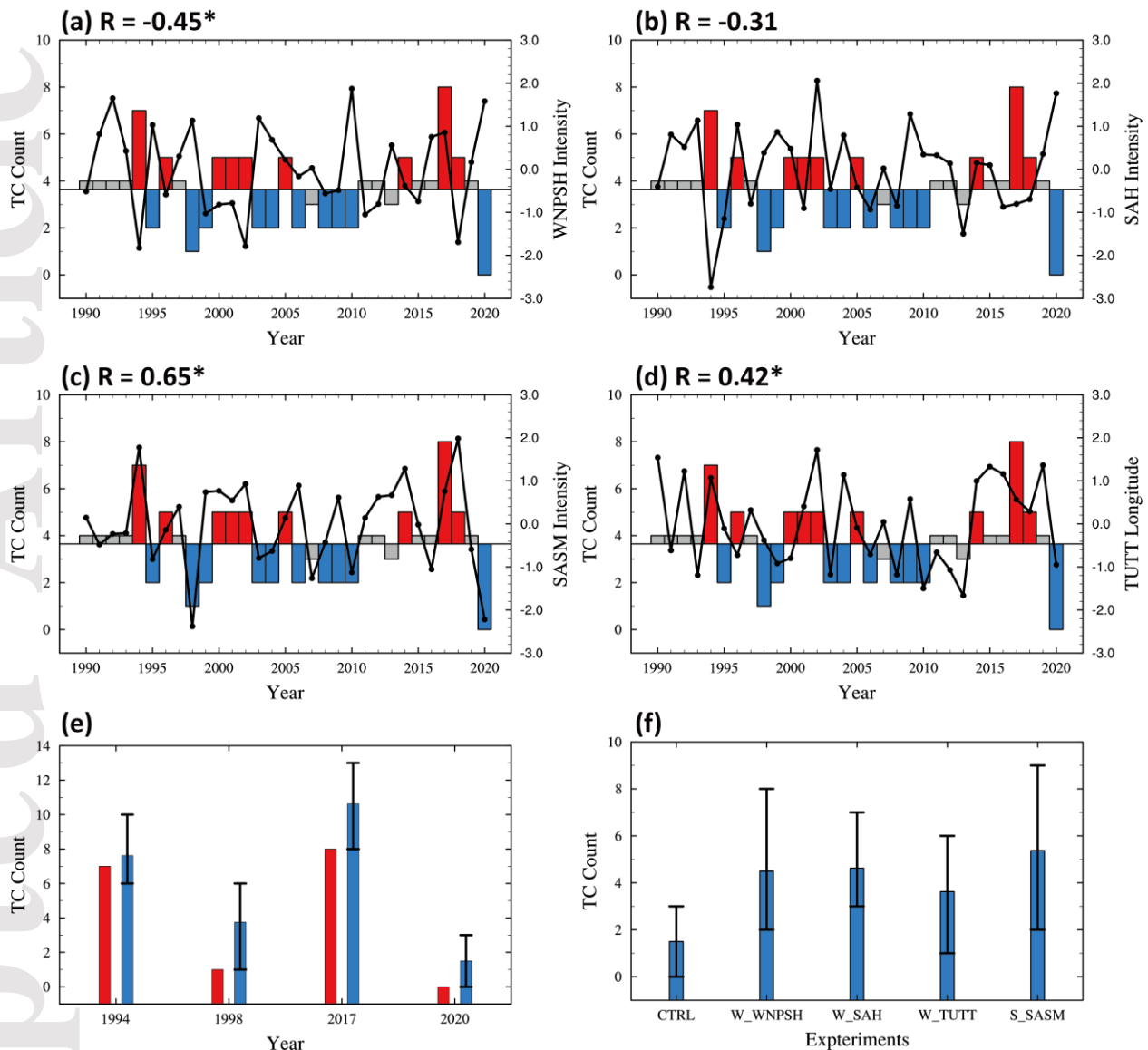


Figure 1. (a-d) Time series of the TC numbers (bars) from the best-track TC data over the WNP in July and the detrended normalized indices (black lines) of the WNPSH, SAH, SASM, and TUTT, respectively, in July from 1990 to 2020, with their correlation coefficients given at the top of their corresponding panels. The star after the correlation coefficient means the correlation exceeds 95% confidence level. The red (blue) bars denote the active (inactive) TC years. (e) TC counts of July from the best track data (red) and ensemble-mean model results (blue) in 1994, 1998, 2017, and 2020, respectively. (f) TC counts from ensemble-mean model results in the experiments of CTRL, W_WNPSH, W_SAH, W_TUTT and S_SASM in July 2020. The thin vertical bars in (e-f) are the ensemble range.

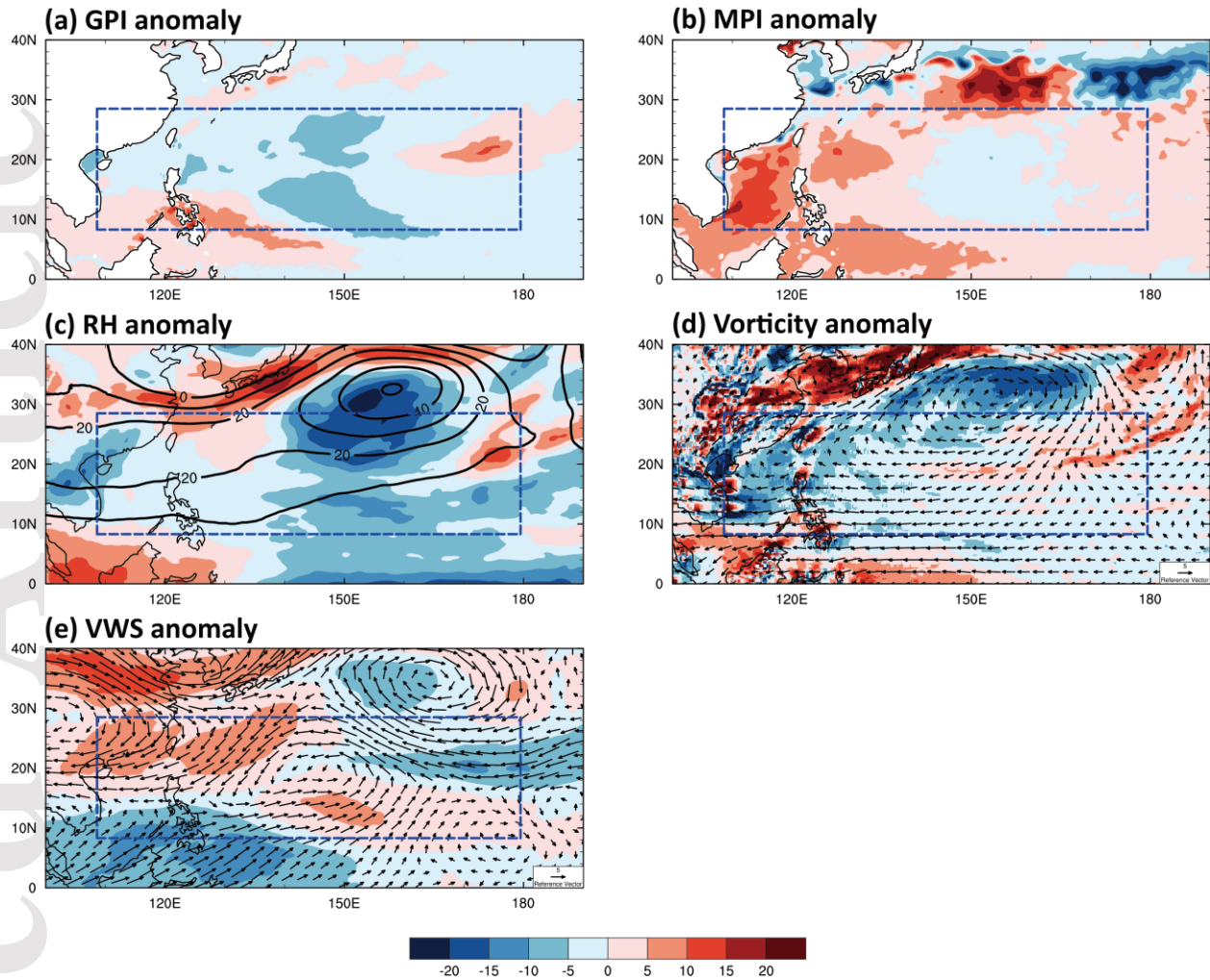


Figure 2. Differences in (a) GPI, (b) MPI (m s^{-1}), (c) 600-hPa RH (shading, %) and 500-hPa geopotential height (contours, 10 gpm), (d) 850-hPa relative vorticity (shading, 10^{-6} s^{-1}) and 850-hPa horizontal winds (vectors, m s^{-1}), and (e) VWS (shading, m s^{-1}) and 200-hPa horizontal winds (vectors, m s^{-1}) between July 2020 and the 31-year July mean. The dashed blue box denotes the potential genesis region (PGR).

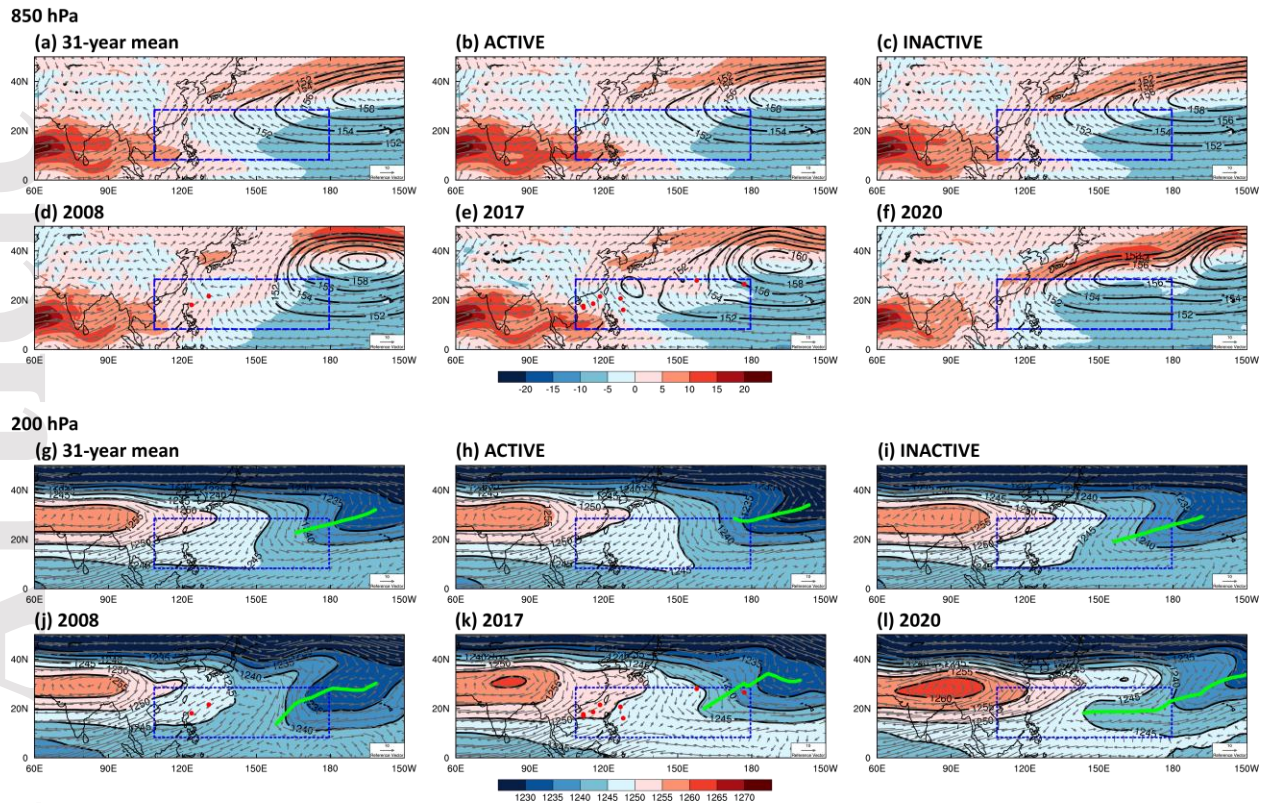


Figure 3. Geopotential height greater than 1520 gpm (contours, 10 gpm), zonal wind speed (shading, m s^{-1}), and horizontal winds (vectors, m s^{-1}) at 850 hPa in July for (a) the 31-year mean, (b) mean active TC years (ACTIVE), (c) mean inactive TC years (INACTIVE), (d) 2008, (e) 2017 and (f) 2020. (g-l) are the same as (a-f) but for geopotential height (contours and shading, 10 gpm) and horizontal winds (vectors, m s^{-1}) at 200 hPa. The red dots denote the locations of TC formation. The green line represents the trough line of TUTT. The dashed blue box denotes the PGR.

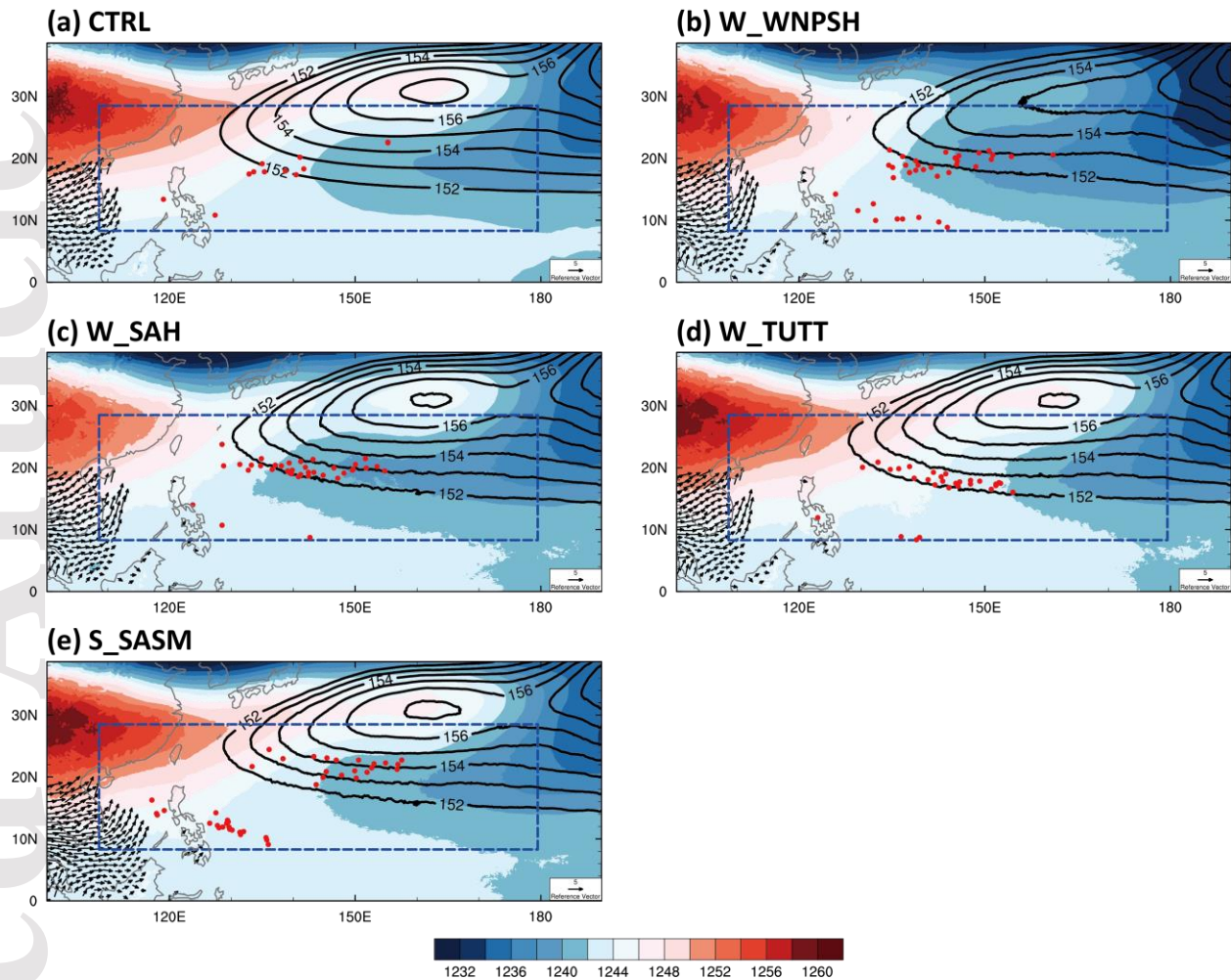


Figure 4. Initial conditions of the WRF model in (a) CTRL, (b) W_WNPSH, (c) W_SAH, (d) W_TUTT, and (e) S_SASM, including horizontal wind with zonal wind greater than 1 m s^{-1} (vectors, m s^{-1}) and geopotential height greater than 1520 gpm (contours, 10 gpm) at 850 hPa, and geopotential height at 200 hPa (shading, 10 gpm). The dashed blue box denotes the PGR. The red dots are the locations of the simulated TC formation in all members.